# Probing on the Stable Structure of Silicon-Doped Charged Magnesium Nanomaterial Sensor: $SiMg_n^{\pm1}$ ($N$ = 2−12) Clusters DFT Study

Lu Zeng[1]*, Xiao-Fan Wei[1], Mei-Kun Liang[1], Jun Zhao[2]* and Ben-Chao Zhu[2]*

[1] College of Materials Science and Engineering, Chongqing University, Chongqing, China, [2] School of Public Health, Hubei University of Medicine, Shiyan, China

The stable structures of silicon-doped charged magnesium nanomaterial sensor, $SiMg_n^{\pm1}$ ($n$ = 2−12) clusters, were systematically investigated using the CALYPSO approach coupled with the density functional theory (DFT). The growth mechanism of $SiMg_n^{\pm1}$ ($n$ = 2−12) nanosensors shows that the tetrahedral and tower-like structures are two basic structures, and almost all other clusters' geometries are based on their variants. Most importantly, the fascinating $SiMg_8^{-1}$ and $SiMg_8^{+1}$ clusters are obtained through stability calculations of all the lowest energy state of clusters. These two clusters show the strongest local stability and thus can be served as reliable candidates for experimentally fabricated silicon-doped magnesium nanosensor. Electronic structural properties and chemical bonding analysis are also adopted to further study the stability of $SiMg_8^{-1}$ and $SiMg_8^{+1}$ nanosensors. The theoretical calculations of infrared (IR) and Raman spectra of $SiMg_8^{-1}$ and $SiMg_8^{+1}$ clusters show that their strongest spectral frequencies are distributed in the range of 80−240 $cm^{-1}$. We believe that our studies will stimulate future synthesis of silicon-doped magnesium in IoT nanosensors.

Keywords: DFT, silicon-doped magnesium, nanomaterial sensor, $SiMg_n^{\pm1}$ clusters, CALYPSO

## INTRODUCTION

Magnesium and silicon, as important optoelectronics and semiconductor sensor materials, have been the frontier of material science (Delgado et al., 2004; Capitán-Vallvey et al., 2006; Wang et al., 2015; Pradeep et al., 2017). With the widespread application of IoT sensors, the development and research of magnesium or silicon sensor at nanoscale with small size and good performance are increasingly sought after by researchers (Shukla et al., 2004; Pham et al., 2014). New nanosensor is one of the types of nanomaterials which can be studied through theoretical or experimental research (Zeng et al., 2012; Guo et al., 2014; Wang et al., 2020). Generally, experimental nanomaterials research often provides some new preparation methods, and experimental measurement of the physical and chemical quantities of materials. While theoretical studies of nanomaterials always tend to report on some new potential materials and calculate their physical and chemical properties. Notably, one of the most significant theoretical studies on the nanomaterials is that these predicating nanostructures must be stable

and experimentally feasible. Fortunately, the atomic clusters is such an interesting and effective approach in theoretically constructing stable nanomaterials. Cluster systems are of extreme interest due to their physical and chemical properties which often vary with the number of atoms they contain, this makes different-sized nanomaterials have different properties.

In recent years, there has been an increasing amount of reports on using atomic clusters together with the first-principle to predict new stable nanomaterials as potential sensors (Ding et al., 2015; Jin et al., 2015, 2016; Xia et al., 2016; Li et al., 2017; Chen et al., 2018; Shao et al., 2019; Zhao et al., 2019; Zhang et al., 2020) such as nanomaterials of Zr-B, Ta-B and Fe-O systems, etc. Nanomaterials of silicon and magnesium are inevitable and are studied through their clusters structures. Specifically, taking silicon-containing nanomaterials as an example, Han and Hagelberg (2001), Han et al. (2002, 2007) used density functional theory (DFT) at B3LYP/LanL2DZ level to study $MoSi_n$ ($n = 1–6$), $Mo_2Si_n$ ($9−16$), and $WSi_n$ ($n = 1–6$, $12$) clusters. Their investigations show that $9MoSi_3$, $Mo_2Si_{10}$, and $WSi_{16}$ clusters have relatively higher stability than others and thus can be served as candidates for their experimental stable nanostructures. In addition, a considerable amount of studies have been reported on magnesium clusters (Köhn et al., 2001; Jellinek and Acioli, 2002; Heidari et al., 2011; Xia et al., 2016). These studies theoretically predicted that $Mg_4$, $Mg_{10}$ and $Mg_{20}$ clusters have relatively stable structures. It is exciting that these stable structures can be obtained through cluster spray experiments and can be used as preparations of their corresponding nanomaterials. It is well known that silicon and magnesium are important and widely used materials, such as semiconductors, building materials, sensors and so on, and magnesium silicide thin film sensor is a very interesting research object. When the research interest in magnesium silicide sensors is transferred to the nanometer size, it becomes very necessary to use cluster methods to study silicon-doped magnesium clusters. Surprisingly, to our best knowledge, except for our previous work on silicon doped neutral magnesium clusters (Zhu et al., 2020), few studies have been made on silicon-doped charged magnesium alloy nanomaterials. In addition, the physical and chemical properties of the clusters will vary with their size and charge. Therefore, studying magnesium clusters doped with silicon-doped cations and anions cannot only help enrich our understanding of silicon-doped magnesium at nanoscale, but can also provide some guidance for future applications. Interestingly, as shown in **Figure 1**, the silicon-doped small-sized anionic and cationic magnesium clusters are also physically equivalent to piezoelectric silicon-doped magnesium clusters. In other words, the piezoelectric state of the $SiMg_n$ cluster can be equivalent to the silicon-doped magnesium nano-piezoelectric sensor to some extent. In short, this paper is to research the silicon-doped magnesium nano piezoelectric sensor and explore their stable structures through density functional theory (DFT) theoretical calculations. The paper is organized as following: Section "Computational Methods" describes the computational methods, the calculation results are reported and completely discussed in Section "Results and Discussions," and the final conclusions can be found in Section "Conclusion."



**FIGURE 1 |** Silicon-doped magnesium nano-ceramic cluster under physical piezoelectric condition.
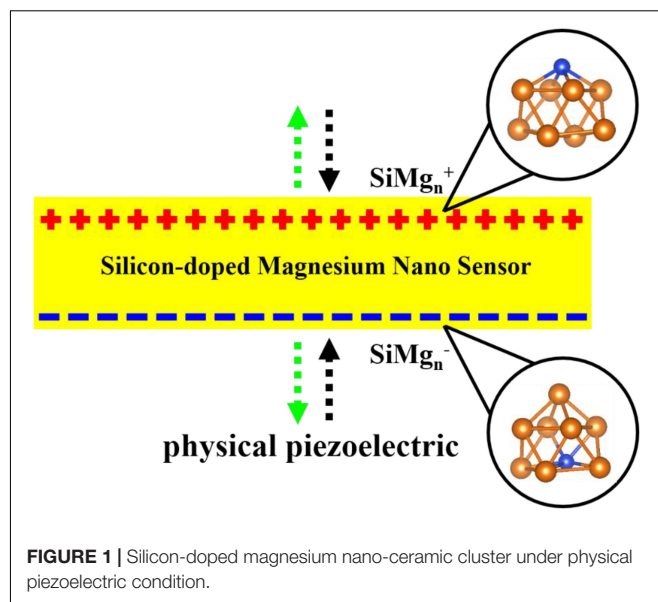
## COMPUTATIONAL METHODS

CALYPSO structure searching code (Wang et al., 2010, 2012; Lv et al., 2012) was adopted to find the structures of low-lying isomers of piezoelectric silicon-doped small-sized magnesium clusters. Several useful structure search techniques, such as symmetry constraints, bond characterization matrix, atom-centered symmetrical function, and structure randomness generation, are included in CALYPSO code. It has been reported that the structures for various systems ranging from clusters to crystal structures have been successfully predicted using CALYPSO (Zhao et al., 2017; Sun et al., 2019; Lin et al., 2020; Lu and Chen, 2020a,b). Here, structure searching is performed for piezoelectric silicon-doped small-sized magnesium clusters up to 13 atoms. Each generation contains 50 structures, 60% of which are generated by CALYPSO's special techniques, and 40% are generated randomly. In order to achieve the convergence of potential energy surface sampling, we followed each cluster for 20 generations. Based on the above search, 1000 structures can be obtained for each $SiMg_n^{\pm 1}$ ($n = 2−12$) cluster. Among these structures, those with low energy and different structures are selected as candidates for subsequent structural optimization calculations. The calculations are performed using density functional theory (DFT) with the hybrid functional B3LYP (Becke, 1988; Lee et al., 1988). The all-electron 6-311G (d) basis set is used to confirmation of the lowest-energy structures of $SiMg_n^{\pm 1}$ ($n = 2−12$) clusters. Taking different spin multiplicities may effect on structures into account, structural optimizations of each isomer of spin multiplicities of 2, 4, 6, and 8 are all implemented. In order to make sure that there is no imaginary frequency affecting the stationary character of state, the harmonic vibration frequency computation is carried out after each structural optimization. All above calculations are performed with the GAUSSIAN 09 program package (Frisch et al., 2009). Natural charge population (NCP), natural electronic

configuration (NEC), molecular orbitals (MOs) and chemical bonding composition are analyzed by natural bond orbital (NBO). Total density of states (TDOS) and partial density of states (PDOS) are calculated and plotted by Multiwfn 3.7 (Lu and Chen, 2012a,b).

The choice of the B3LYP/6-311G(d) lev9el can be explained by **Table 1**, which presents the theoretical calculations results of the bound length ($r$), vibrational frequency ($\omega$) of $Si_2$, $Mg_2$ and SiMg dimers by different functional and basis sets. Compared with experiments (Huber and Herzberg, 1979; Ruette et al., 2005), it can be safely concluded that B3LYP/6-311G(d) combination is an effective choice.

## RESULTS AND DISCUSSION

### Geometrical Structures of SiMg$_n^{\pm 1}$ Nanosensors

The global minima structures of SiMg$_n^{\pm 1}$ ($n = 2-12$) clusters together with the corresponding symmetry, electronic state were obtained using the methods mentioned in Section "Computational Methods," and displayed in **Figure 2** and **Table 2**. The harmonic vibration frequency results of each structure are presented in **Table 2**, which can confirm that there is no imaginary frequency in these structures. Physically, the optimized structures can be regarded as the lowest-energy state structures of piezoelectric silicon-doped magnesium nanomaterials. The geometric analysis of the growth mechanism of these structures will be presented shortly below.

As shown in **Figure 2**, SiMg$_2^{-1}$ and SiMg$_n^{+1}$ clusters have the same isosceles triangle structure. While both SiMg$_3^{-1}$ and SiMg$_3^{+1}$ clusters have the similar tetrahedral structure. For $n = 4-12$, the lowest energy structures of SiMg$_n^{\pm 1}$ clusters differ from each other, which suggests that cationization and anionization have different effects on the structure of silicon-doped magnesium clusters. Moreover, except for the SiMg$_5^{-1}$cluster, which is a plane structure, all other clusters structures are three-dimensional (3D). Interestingly, it can be seen that some relative large-sized SiMg$_n^{\pm 1}$ clusters can be directly formed by small-sized SiMg$_{n-1}^{\pm 1}$ clusters attracting one magnesium atom in different orientation, such as SiMg$_4^{-1}$ and SiMg$_3^{-1}$, SiMg$_9^{-1}$ and SiMg$_8^{-1}$, SiMg$_{12}^{-1}$ and SiMg$_{11}^{-1}$, SiMg$_4^{+1}$ and SiMg$_3^{+1}$, SiMg$_5^{+1}$ and SiMg$_4^{+1}$,

SiMg$_9^{+1}$and SiMg$_8^{+1}$, SiMg$_{10}^{+1}$and SiMg$_9^{+1}$. SiMg$_6^{+1}$ and SiMg$_7^{+1}$ displays relative irregular geometries and they cannot be formed by SiMg$_5^{+1}$and SiMg$_6^{+1}$ attracting one Mg atom. The similar situation also happens in SiMg$_{10}^{-1}$, SiMg$_{11}^{+1}$ and SiMg$_{12}^{+1}$, which show a little more complicated, and cannot be directly obtained by smaller size clusters of SiMg$_9^{-1}$, SiMg$_{10}^{+1}$ and SiMg$_{11}^{+1}$. However, these clusters can be considered to be based on the deformation of the tetrahedron (SiMg$_3^{\pm 1}$) and a kind of tower (such as SiMg$_8^{-1}$, but not the atoms fixed in this position). It is necessary to point out that this type of structure growth mechanism is not discovered for the first time, and has been confirmed to exist in the previous reports of metal alloy cluster studies (Xia et al., 2016; Li et al., 2017; Chen et al., 2018; Zhao et al., 2019). However, it is worth noting that SiMg$_8^{-1}$ and SiMg$_8^{+1}$ clusters are special ones due to their tower-like structures. For $n = 9-12$, all SiMg$_n^{\pm 1}$ clusters structures are tower-like-based structures originated from the transformation of SiMg$_8^{\pm 1}$ structures. The following studies will show that the specificity of SiMg$_8^{-1}$ and SiMg$_8^{+1}$ clusters is not only exist in geometric structure, but also physical and chemical properties.

### Electronic Properties of the Ground State of SiMg$_n^{\pm 1}$ Nanosensors

The studies of electronic properties of clusters, such as the natural charge population (NCP), natural electronic configuration (NEC), help us further understand the structures formation. The NCP and NEC of the ground state of SiMg$_n^{\pm 1}$ ($n = 2-12$) clusters were analyzed by the natural bond orbital (NBO) (Reed et al., 1988a,b), and displayed in **Tables 3–6**. It can be seen from **Tables 3**, **4** that Si atoms are all negatively charged in all of SiMg$_n^{\pm 1}$ ($n = 2-12$) clusters, while most Mg atoms are positively charged. To better understand the effect of silicon doping on the charge transfer of magnesium clusters, the total charges on silicon atoms in the ground state of SiMg$_n^{\pm 1}$ ($n = 2-12$) clusters were presented in **Figure 3**. As shown in **Figure 3**, the Si atom charge overall decreases in both SiMg$_n^{\pm 1}$ clusters as n increases and the maximal values can be found at SiMg$_7^{-1}$ and SiMg$_8^{+1}$, respectively. The local strong peaks of SiMg$_7^{-1}$ and SiMg$_8^{+1}$ indicate that the beryllium atoms are relatively difficult to get electrons in their structure, so when beryllium is doped into magnesium clusters, it is easy to be adsorbed on the surface of the

**TABLE 1 |** Calculated values of bond length r (Å), frequency $\omega$ (cm$^{-1}$) for $Si_2$, $Mg_2$, and SiMg isomers using different methods.

| Methods | Si$_2$ | | Mg$_2$ | | SiMg | |
|---|---|---|---|---|---|---|
| | r (Å) | $\omega$ (cm$^{-1}$) | r (Å) | $\omega$ (cm$^{-1}$) | r (Å) | $\omega$ (cm$^{-1}$) |
| B3LYP/6-311G(d) | 2.17 | 540.82 | 3.93 | 44.96 | 2.57 | 288.31 |
| B3PW91/6-311G(d) | 2.31 | 476.71 | 3.61 | 85.29 | 2.54 | 325.98 |
| PBE/6-311G(d) | 2.18 | 531.49 | 2.78 | 263.51 | 2.56 | 311.01 |
| BPV86/6-311G(d) | 2.18 | 527.65 | 2.78 | 259.56 | 2.55 | 306.74 |
| MP1PW91/6-311G(d) | 2.30 | 484.06 | 3.60 | 88.05 | 2.54 | 327.96 |
| Expt | 2.25[a] | 511.00[a] | 3.89[b] | 45.00[b] | — | — |

[a]Huber and Herzberg (1979); [b]Ruette et al. (2005).
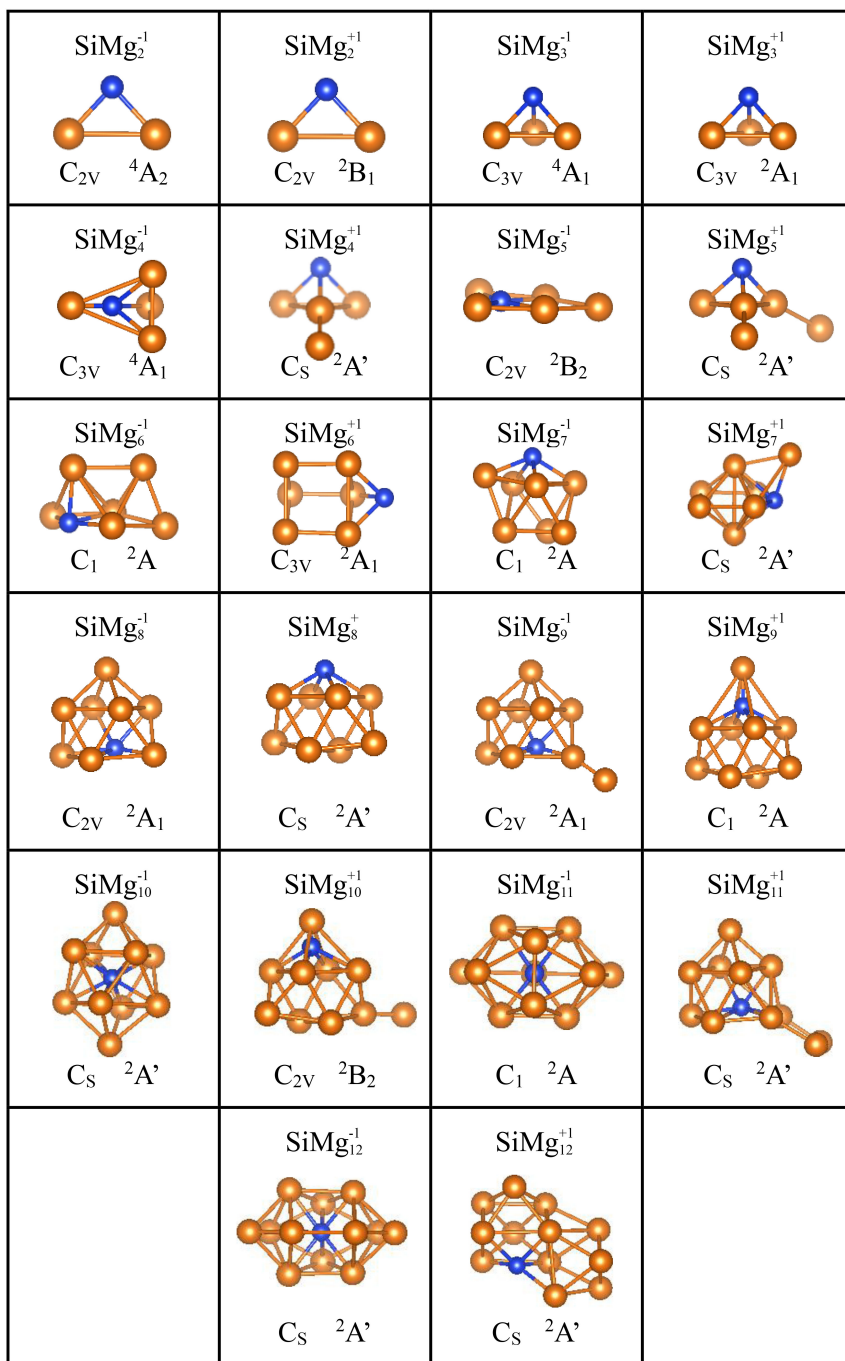
**FIGURE 2 |** Optimized geometrical structures of ground state of $SiMg_n^{\pm 1}$ ($n$ = 2–12) clusters at B3LYP /6-311+G(d) level. The yellow and blue balls are magnesium and silicon atoms, respectively.

structure, and the geometric structures of $SiMg_7^{-1}$ and $SiMg_8^{+1}$ in **Figure 2** confirms this conclusion. NCP shows that the charges are transferred from Mg atoms to Si atoms in $SiMg_n^{\pm 1}$ ($n$ = 2−12) clusters. Si atom acts as charge receiver while the Mg atoms are charge donors is probably originated from the fact that electronegativity value of Si (1.90) is greater than that of Mg atom (1.31).

**Tables 5**, **6** present the NEC in the lowest-energy states of $SiMg_n^{\pm 1}$ ($n$ = 2−12) clusters. Compared with the NEC of the isolated Si ($3s^2 3p^2$) and Mg ($3s^2$) atoms, one can find that Si and Mg atoms lose electrons in 3s-orbital and gain electrons in 3p-orbitals in $SiMg_n^{\pm 1}$ ($n$ = 2−12) clusters. Quantitatively, as can be seen from **Tables 5**, **6**, the Si 3s-orbital of $SiMg_n^{-1}$ clusters lost electrons is in the range of 0.13 to 0.44 electrons,

**TABLE 2** | NCP of the ground state of $SiMg_n^{-1}$ ($n$ = 2–12) clusters.

| Number of Mg atoms | Anionic | | | | | | | | | Cationic | | | | | | | | |
|---|---|---|---|---|---|---|---|---|---|---|---|---|---|---|---|---|---|---|
| | Symm | Stat | $E_b$ (eV) | $E_f$ (eV) | $\Delta_2E$ (eV) | $\alpha E_{gap}$ (eV) | $\beta E_{gap}$ (eV) | Frequencies (cm$^{-1}$) | | Symm | Stat | $E_b$ (eV) | $E_f$ (eV) | $\Delta_2E$ (eV) | $\alpha E_{gap}$ (eV) | $\beta E_{gap}$ (eV) | Frequencies (cm$^{-1}$) | |
| | | | | | | | | Highest | Lowest | | | | | | | | Highest | Lowest |
| 2 | $C_{2V}$ | $^4A_2$ | 1.54 | – | – | 2.29 | 2.79 | 256.19 | 58.69 | $C_{2V}$ | $^2B_1$ | 1.58 | – | – | 2.16 | 3.28 | 306.42 | 101.85 |
| 3 | $C_{3V}$ | $^4A_1$ | 1.36 | 0.82 | 0.31 | 2.29 | 2.95 | 272.60 | 68.21 | $C_{3V}$ | $^2A_1$ | 1.45 | 1.07 | 0.41 | 1.42 | 3.58 | 307.30 | 80.40 |
| 4 | $C_{3V}$ | $^4A_1$ | 1.19 | 0.51 | 0.01 | 2.24 | 1.94 | 281.23 | 21.78 | $C_S$ | $^2A'$ | 1.29 | 0.66 | 0.15 | 1.20 | 2.84 | 333.10 | 41.24 |
| 5 | $C_{2V}$ | $^2B_2$ | 1.07 | 0.50 | 0.11 | 1.58 | 1.57 | 317.01 | 28.05 | $C_S$ | $^2A'$ | 1.16 | 0.51 | −0.01 | 1.03 | 2.79 | 337.35 | 22.96 |
| 6 | $C_1$ | $^2A$ | 0.98 | 0.39 | −0.45 | 1.45 | 1.32 | 304.65 | 28.01 | $C_{3V}$ | $^2A_1$ | 1.07 | 0.52 | 0.01 | 1.69 | 2.17 | 335.24 | 52.45 |
| 7 | $C_S$ | $^2A''$ | 0.96 | 0.84 | 0.04 | 1.54 | 1.45 | 301.08 | 17.52 | $C_1$ | $^2A$ | 1.00 | 0.51 | −0.47 | 1.77 | 1.70 | 268.70 | 24.01 |
| 8 | $C_S$ | $^2A''$ | 0.94 | 0.80 | 0.53 | 1.22 | 1.80 | 299.50 | 54.67 | $C_{2V}$ | $^2A_1$ | 1.00 | 0.98 | 0.30 | 2.10 | 1.55 | 284.53 | 82.69 |
| 9 | $C_1$ | $^2A$ | 0.87 | 0.27 | −0.26 | 1.15 | 1.79 | 311.39 | 22.20 | $C_{2V}$ | $^2A_1$ | 0.97 | 0.68 | 0.36 | 1.78 | 1.92 | 315.38 | 35.46 |
| 10 | $C_{2V}$ | $^2B_2$ | 0.84 | 0.53 | 0.10 | 1.54 | 0.97 | 322.08 | 27.59 | $C_S$ | $^2A'$ | 0.91 | 0.33 | −0.10 | 1.64 | 1.79 | 320.29 | 22.89 |
| 11 | $C_S$ | $^2A'$ | 0.81 | 0.43 | −0.04 | 1.19 | 1.53 | 335.75 | 22.00 | $C_1$ | $^2A$ | 0.87 | 0.42 | −0.06 | 1.51 | 1.70 | 330.94 | 24.98 |
| 12 | $C_S$ | $^2A'$ | 0.78 | 0.46 | – | 1.41 | 1.13 | 335.30 | 28.15 | $C_S$ | $^2A'$ | 0.84 | 0.48 | – | 1.23 | 1.73 | 320.15 | 30.26 |

**TABLE 3** | NCP of the ground state of $SiMg_n^{+1}$ ($n$ = 2–12) clusters.

| Clusters | Si-1 | Mg-2 | Mg-3 | Mg-4 | Mg-5 | Mg-6 | Mg-7 | Mg-8 | Mg-9 | Mg-10 | Mg-11 | Mg-12 | Mg-13 |
|---|---|---|---|---|---|---|---|---|---|---|---|---|---|
| SiMg−1 2 | −1.13 | 0.06 | 0.06 | | | | | | | | | | |
| SiMg−1 3 | −1.60 | 0.20 | 0.20 | 0.20 | | | | | | | | | |
| SiMg−1 4 | −2.15 | 0.31 | 0.31 | 0.31 | 0.24 | | | | | | | | |
| SiMg−1 5 | −1.98 | 0.38 | 0.38 | 0.06 | 0.09 | 0.06 | | | | | | | |
| SiMg−1 6 | −1.77 | 0.24 | 0.35 | −0.07 | −0.05 | 0.35 | −0.03 | | | | | | |
| SiMg−1 7 | −1.59 | 0.27 | −0.09 | 0.18 | 0.18 | −0.09 | −0.09 | 0.24 | | | | | |
| SiMg−1 8 | −1.79 | −0.08 | 0.10 | −0.01 | 0.27 | −0.08 | 0.15 | 0.15 | 0.27 | | | | |
| SiMg−1 9 | −1.76 | −0.01 | −0.07 | 0.01 | −0.01 | 0.14 | 0.28 | 0.23 | 0.13 | 0.06 | | | |
| SiMg−1 10 | −2.69 | 0.21 | 0.21 | 0.16 | 0.16 | 0.07 | 0.20 | 0.07 | 0.20 | 0.20 | 0.20 | | |
| SiMg−1 11 | −2.68 | 0.13 | 0.17 | 0.13 | 0.17 | 0.40 | 0.09 | 0.12 | 0.12 | 0.10 | 0.08 | 0.17 | |
| SiMg−1 12 | −2.54 | 0.29 | 0.03 | 0.10 | 0.04 | 0.06 | 0.23 | 0.29 | 0.26 | 0.23 | 0.06 | 0.12 | −0.16 |

**TABLE 4 |** NEC of the ground state of $SiMg_n^{-1}$ ($n$ = 2–12) clusters.

| Clusters | Si-1 | Mg-2 | Mg-3 | Mg-4 | Mg-5 | Mg-6 | Mg-7 | Mg-8 | Mg-9 | Mg-10 | Mg-11 | Mg-12 | Mg-13 |
|---|---|---|---|---|---|---|---|---|---|---|---|---|---|
| SiMg+1 2 | −0.59 | 0.80 | 0.80 | | | | | | | | | | |
| SiMg+1 3 | −1.13 | 0.71 | 0.71 | 0.71 | | | | | | | | | |
| SiMg+1 4 | −1.18 | 0.40 | 0.66 | 0.66 | 0.46 | | | | | | | | |
| SiMg+1 5 | −1.24 | 0.39 | 0.41 | 0.63 | 0.41 | 0.39 | | | | | | | |
| SiMg+1 6 | −1.22 | 0.57 | 0.17 | 0.57 | 0.17 | 0.57 | 0.17 | | | | | | |
| SiMg+1 7 | −1.74 | 0.23 | 0.23 | 0.56 | 0.02 | 0.35 | 0.77 | 0.58 | | | | | |
| SiMg+1 8 | −1.30 | 0.29 | 0.04 | 0.41 | 0.41 | 0.04 | 0.41 | 0.29 | 0.41 | | | | |
| SiMg+1 9 | −2.13 | 0.05 | 0.30 | 0.42 | 0.42 | 0.30 | 0.42 | 0.42 | 0.05 | 0.74 | | | |
| SiMg+1 10 | −2.13 | 0.44 | 0.27 | 0.11 | 0.46 | 0.45 | 0.44 | 0.11 | 0.73 | −0.32 | 0.45 | | |
| SiMg+1 11 | −2.11 | 0.21 | 0.54 | 0.56 | −0.05 | 0.29 | 0.32 | 0.39 | 0.25 | 0.23 | 0.04 | 0.33 | |
| SiMg+1 12 | −1.95 | 0.41 | 0.56 | 0.26 | 0.48 | 0.26 | 0.48 | 0.41 | −0.16 | −0.07 | −0.07 | 0.29 | 0.10 |

**TABLE 5 |** NEC of the ground state of $SiMg_n^{+1}$ ($n$ = 2–12) clusters.

| Clusters | Si-1 | Mg-2 | Mg-3 | Mg-4 | Mg-5 | Mg-6 | Mg-7 | Mg-8 | Mg-9 | Mg-10 | Mg-11 | Mg-12 | Mg-13 |
|---|---|---|---|---|---|---|---|---|---|---|---|---|---|
| SiMg−1 2 | $3S^{1.87}3p^{3.25}$ | $3S^{1.53}3p^{0.39}$ | $3S^{1.53}3p^{0.39}$ | | | | | | | | | | |
| SiMg−1 3 | $3S^{1.80}3p^{3.79}$ | $3S^{1.37}3p^{0.41}$ | $3S^{1.37}3p^{0.41}$ | $3S^{1.37}3p^{0.41}$ | | | | | | | | | |
| SiMg−1 4 | $3S^{1.82}3p^{4.32}$ | $3S^{1.40}3p^{0.28}$ | $3S^{1.40}3p^{0.28}$ | $3S^{1.40}3p^{0.28}$ | $3S^{1.58}3p^{0.17}$ | | | | | | | | |
| SiMg−1 5 | $3S^{1.70}3p^{4.27}$ | $3S^{1.26}3p^{0.35}$ | $3S^{1.26}3p^{0.35}$ | $3S^{1.20}3p^{0.72}$ | $3S^{1.48}3p^{0.42}$ | $3S^{1.20}3p^{0.72}$ | | | | | | | |
| SiMg−1 6 | $3S^{1.71}3p^{4.04}$ | $3S^{1.11}3p^{0.63}$ | $3S^{1.17}3p^{0.47}$ | $3S^{1.13}3p^{0.92}$ | $3S^{1.45}3p^{0.59}$ | $3S^{1.35}3p^{0.29}$ | $3S^{1.35}3p^{0.67}$ | | | | | | |
| SiMg−1 7 | $3S^{1.67}3p^{3.91}$ | $3S^{1.20}3p^{0.63}$ | $3S^{1.26}3p^{0.82}$ | $3S^{1.13}3p^{0.67}$ | $3S^{1.13}3p^{0.67}$ | $3S^{1.26}3p^{0.82}$ | $3S^{1.24}3p^{0.83}$ | $3S^{1.13}3p^{0.67}$ | | | | | |
| SiMg−1 8 | $3S^{1.62}3p^{4.15}$ | $3S^{1.19}3p^{0.87}$ | $3S^{1.15}3p^{0.73}$ | $3S^{1.18}3p^{0.82}$ | $3S^{1.12}3p^{0.59}$ | $3S^{1.19}3p^{0.87}$ | $3S^{1.07}3p^{0.75}$ | $3S^{1.07}3p^{0.75}$ | $3S^{1.12}3p^{0.59}$ | | | | |
| SiMg−1 9 | $3S^{1.61}3p^{4.14}$ | $3S^{1.09}3p^{0.89}$ | $3S^{1.16}3p^{0.89}$ | $3S^{1.17}3p^{0.81}$ | $3S^{1.17}3p^{0.81}$ | $3S^{1.14}3p^{0.70}$ | $3S^{1.11}3p^{0.59}$ | $3S^{1.04}3p^{0.70}$ | $3S^{1.09}3p^{0.76}$ | $3S^{1.72}3p^{0.21}$ | | | |
| SiMg−1 10 | $3S^{1.60}3p^{5.06}$ | $3S^{1.13}3p^{0.63}$ | $3S^{1.13}3p^{0.63}$ | $3S^{1.12}3p^{0.70}$ | $3S^{1.12}3p^{0.70}$ | $3S^{1.27}3p^{0.64}$ | $3S^{1.12}3p^{0.65}$ | $3S^{1.24}3p^{0.67}$ | $3S^{1.12}3p^{0.65}$ | $3S^{1.12}3p^{0.65}$ | $3S^{1.12}3p^{0.65}$ | | |
| SiMg−1 11 | $3S^{1.58}3p^{5.07}$ | $3S^{1.15}3p^{0.69}$ | $3S^{1.05}3p^{0.76}$ | $3S^{1.15}3p^{0.69}$ | $3S^{1.05}3p^{0.76}$ | $3S^{1.09}3p^{0.48}$ | $3S^{1.26}3p^{0.63}$ | $3S^{1.06}3p^{0.80}$ | $3S^{1.06}3p^{0.80}$ | $3S^{1.26}3p^{0.63}$ | $3S^{1.30}3p^{0.50}$ | $3S^{1.31}3p^{0.51}$ | |
| SiMg−1 12 | $3S^{1.56}3p^{4.96}$ | $3S^{1.00}3p^{0.68}$ | $3S^{0.97}3p^{0.98}$ | $3S^{1.14}3p^{0.74}$ | $3S^{1.15}3p^{0.79}$ | $3S^{1.12}3p^{0.79}$ | $3S^{1.02}3p^{0.73}$ | $3S^{1.00}3p^{0.68}$ | $3S^{1.35}3p^{0.38}$ | $3S^{1.02}3p^{0.73}$ | $3S^{1.12}3p^{0.79}$ | $3S^{1.26}3p^{0.60}$ | $3S^{1.22}3p^{0.93}$ |

**TABLE 6 |** State, symmetry, $E_b$, $E_f$, $\Delta_2 E$, $E_{gap}$, and vibrational frequencies of the ground state of SiMg$_n^{\pm 1}$ (n = 2−12) clusters.

| Clusters | Si-1 | Mg-2 | Mg-3 | Mg-4 | Mg-5 | Mg-6 | Mg-7 | Mg-8 | Mg-9 | Mg-10 | Mg-11 | Mg-12 | Mg-13 |
|---|---|---|---|---|---|---|---|---|---|---|---|---|---|
| SiMg+1 2 | $3S^{1.91}3p^{2.67}$ | $3S^{1.08}3p^{0.11}$ | | | | | | | | | | | |
| SiMg+1 3 | $3S^{1.85}3p^{3.25}$ | $3S^{1.08}3p^{0.18}$ | $3S^{1.08}3p^{0.11}$ | | | | | | | | | | |
| SiMg+1 4 | $3S^{1.81}3p^{3.36}$ | $3S^{1.06}3p^{0.52}$ | $3S^{1.08}3p^{0.18}$ | $3S^{1.08}3p^{0.18}$ | | | | | | | | | |
| SiMg+1 5 | $3S^{1.78}3p^{3.45}$ | $3S^{1.08}3p^{0.51}$ | $3S^{1.13}3p^{0.21}$ | $3S^{1.11}3p^{0.21}$ | $3S^{1.51}3p^{0.02}$ | | | | | | | | |
| SiMg+1 6 | $3S^{1.75}3p^{3.46}$ | $3S^{0.93}3p^{0.41}$ | $3S^{1.55}3p^{0.03}$ | $3S^{1.13}3p^{0.21}$ | $3S^{1.55}3p^{0.03}$ | $3S^{1.08}3p^{0.51}$ | | | | | | | |
| SiMg+1 7 | $3S^{1.74}3p^{3.98}$ | $3S^{1.19}3p^{0.57}$ | $3S^{1.42}3p^{0.39}$ | $3S^{0.93}3p^{0.41}$ | $3S^{1.42}3p^{0.39}$ | $3S^{0.93}3p^{0.41}$ | $3S^{1.42}3p^{0.39}$ | | | | | | |
| SiMg+1 8 | $3S^{1.69}3p^{3.60}$ | $3S^{1.18}3p^{0.52}$ | $3S^{1.16}3p^{0.78}$ | $3S^{1.12}3p^{0.31}$ | $3S^{1.03}3p^{0.91}$ | $3S^{1.05}3p^{0.47}$ | $3S^{1.05}3p^{0.15}$ | $3S^{1.07}3p^{0.28}$ | | | | | |
| SiMg+1 9 | $3S^{1.67}3p^{4.44}$ | $3S^{1.13}3p^{0.80}$ | $3S^{1.19}3p^{0.50}$ | $3S^{0.95}3p^{0.61}$ | $3S^{0.95}3p^{0.61}$ | $3S^{1.16}3p^{0.78}$ | $3S^{0.95}3p^{0.61}$ | $3S^{1.18}3p^{0.52}$ | $3S^{0.95}3p^{0.61}$ | | | | |
| SiMg+1 10 | $3S^{1.67}3p^{4.44}$ | $3S^{0.99}3p^{0.56}$ | $3S^{1.22}3p^{0.49}$ | $3S^{1.10}3p^{0.77}$ | $3S^{1.52}3p^{0.02}$ | $3S^{0.91}3p^{0.61}$ | $3S^{0.99}3p^{0.56}$ | $3S^{0.97}3p^{0.59}$ | $3S^{1.17}3p^{0.09}$ | $3S^{1.17}3p^{0.08}$ | | | |
| SiMg+1 11 | $3S^{1.63}3p^{4.46}$ | $3S^{1.11}3p^{0.67}$ | $3S^{1.03}3p^{0.43}$ | $3S^{1.01}3p^{0.41}$ | $3S^{1.02}3p^{1.01}$ | $3S^{1.15}3p^{0.53}$ | $3S^{1.15}3p^{0.65}$ | $3S^{1.40}3p^{0.20}$ | $3S^{1.45}3p^{0.29}$ | $3S^{1.01}3p^{0.74}$ | $3S^{1.12}3p^{0.83}$ | | |
| SiMg+1 12 | $3S^{1.62}3p^{4.31}$ | $3S^{1.07}3p^{0.51}$ | $3S^{1.00}3p^{0.42}$ | $3S^{1.16}3p^{0.56}$ | $3S^{0.96}3p^{0.64}$ | $3S^{1.16}3p^{0.56}$ | $3S^{1.07}3p^{0.51}$ | $3S^{1.07}3p^{0.51}$ | $3S^{1.16}3p^{1.18}$ | $3S^{0.90}3p^{1.15}$ | $3S^{0.90}3p^{1.15}$ | $3S^{1.10}3p^{0.60}$ | $3S^{1.13}3p^{0.76}$ |
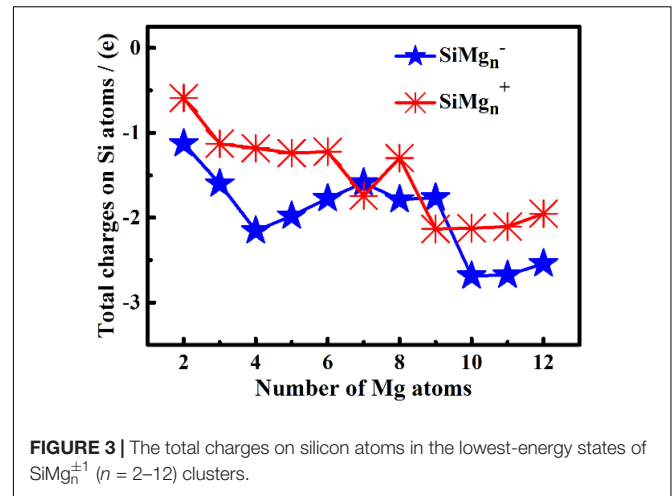


**FIGURE 3 |** The total charges on silicon atoms in the lowest-energy states of SiMg$_n^{\pm 1}$ (n = 2–12) clusters.

while that of SiMg$_n^{+1}$ clusters ranges from 0.09 to 0.38 electrons. Correspondingly, the Si 3p-orbitals of SiMg$_n^{-1}$ clusters gained electrons ranges from 1.25 to 3.07 electrons, and that of SiMg$_n^{+1}$ clusters is in the range of 0.67 to 2.46 electrons. A significant conclusion is that Si atom in SiMg$_n^{-1}$ clusters gain and lose electrons is easier than the Si atom in SiMg$_n^{+1}$ clusters. Based on the analysis above, the lowest-energy states of SiMg$_n^{\pm 1}$ (n = 2−12) clusters structures are mainly governed by the s- and p-orbitals interactions of Si and Mg atoms.

## The Relative Stability of SiMg$_n^{\pm 1}$ Nanosensors

The study of the relative stability of different sized clusters can reveal which clusters are most stable locally, which can further guide experiments to synthesize these stable clusters. The average binding energy $E_b$, fragmentation energy $E_f$ and the second-order energy difference $\Delta_2 E$ and HOMO-LUMO gap of the lowest energy states were calculated to research the relative stability of SiMg$_n^{\pm 1}$ (n = 2−12) clusters. The results are summarized in **Table 2** and are plotted in **Figures 4, 5**. Their equations are as follows:

$$E_b(SiMg_n^{-1/+1}) = [(n-1)E_k(Mg^{-1/+1}) +$$

$$E_k(Si) - E_k(SiMg_{n-1}^{-1/+1})]/(n+1) \qquad (1)$$

$$E_f(SiMg_n^{-1/+1}) = E_k(SiMg_{n-1}^{-1/+1}) +$$

$$E_k(Mg) - E_k(SiMg_n^{-1/+1}) \qquad (2)$$

$$\Delta_2 E(SiMg_n^{-1/+1}) = E_k(SiMg_{n+1}^{-1/+1}) + E_k(SiMg_{n-1}^{-1/+1}) -$$

$$2E_k(SiMg_n^{-1/+1}) \qquad (3)$$

$E_k$ in Eq. (1) − Eq. (3) are the total energy of the corresponding atom and clusters.

FIGURE 4 | Size-dependent properties of panels (A) $E_b$, (B) $E_f$, and (C) $\Delta_2 E$ for the ground state of $SiMg_n^{\pm 1}$ ($n = 2-12$) clusters.



FIGURE 5 | HOMO-LUMO energy gap of α and β electrons in ground state of panels (A) $E_{gap}$ for $SiMg_n^{-1}$, (B) $E_{gap}$ for $SiMg_n^{+1}$ ($n = 2-12$) clusters.
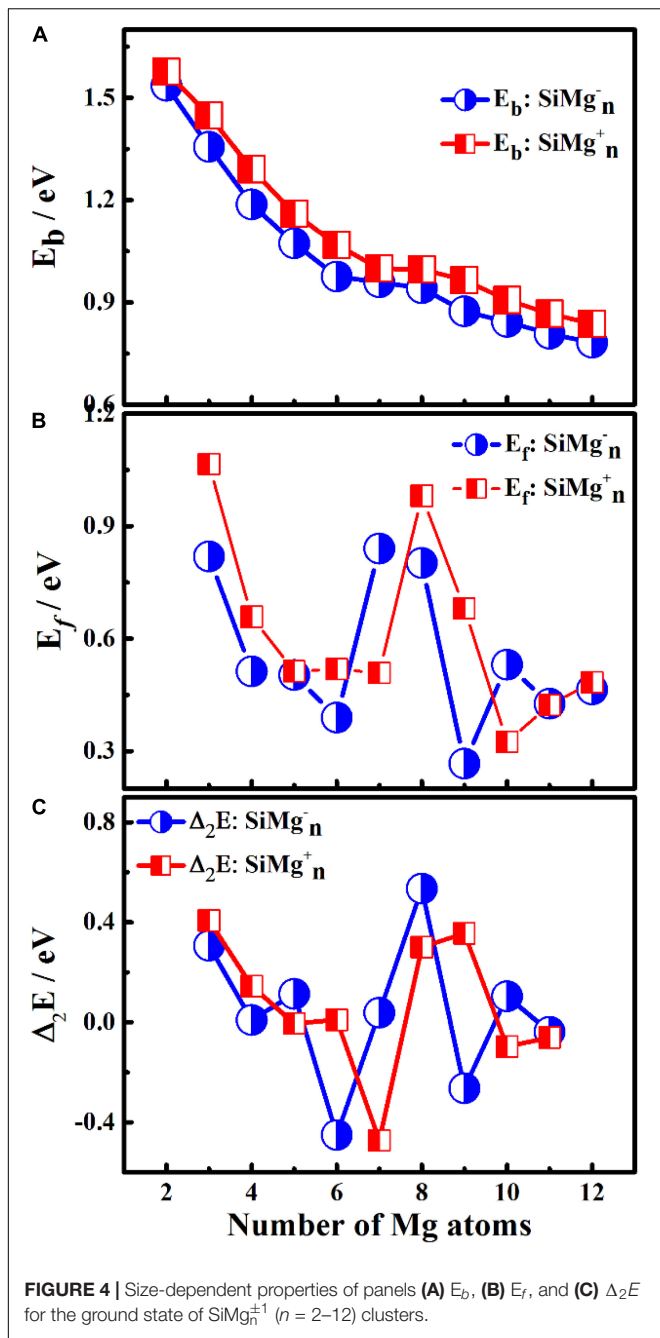
As can be seen from **Figure 4A**, the $E_b$ of $SiMg_n^{\pm 1}$ ($n = 2-12$) clusters have the same size dependence, which decrease with the cluster size. Only two local weak peaks at $SiMg_8^{-1}$ and $SiMg_8^{+1}$ are found, which indicates that these clusters are more stable than their adjacent clusters. Moreover, the $E_b$ values of $SiMg_n^{+1}$ clusters are always higher than that of the corresponding $SiMg_n^{-1}$, which reveals that $SiMg_n^{+1}$ clusters are more stable than the corresponding $SiMg_n^{-1}$. The fragmentation energy $E_f$ can measure the energy of a small-sized cluster adsorbs a related atom to become a larger-sized cluster, which changes with the size and electronic structure of the cluster. A larger local
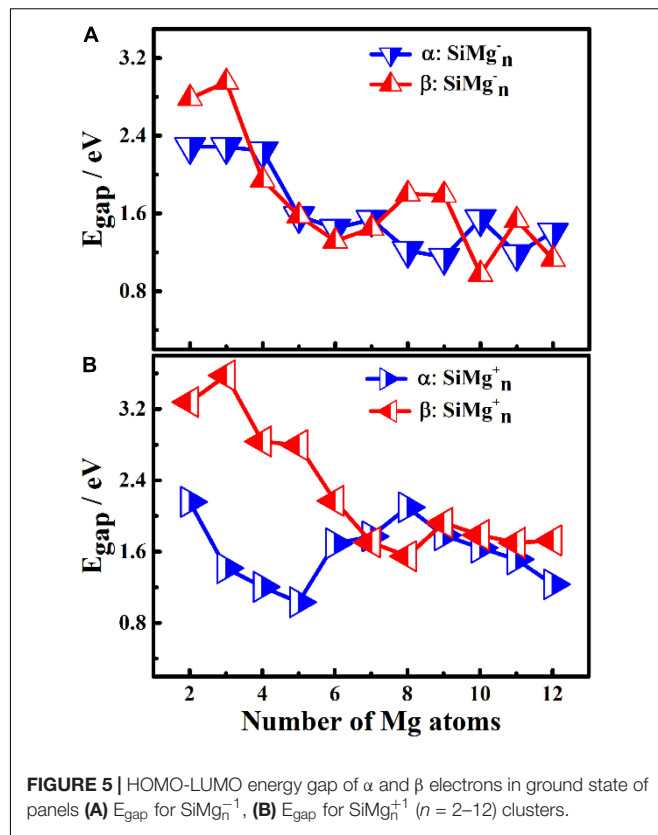
$E_f$ value indicates that the energy required to break the bond between the atoms of the cluster is greater, and correspondingly indicates that the cluster is more stable than its neighboring clusters. **Figure 4B** shows the $E_f$ of $SiMg_n^{\pm 1}$ ($n = 2-12$) clusters, and two $E_f$ curves display similar oscillation behavior, except for $n = 7$ and 10. The local most stable structures are $SiMg_7^{-1}$, $SiMg_8^{-1}$, $SiMg_{10}^{-1}$, $SiMg_8^{+1}$. It is worth pointing out that the $E_f$ value of $SiMg_8^{-1}$ (0.80 eV) is only slightly lower than that of $SiMg_7^{-1}$ (0.84 eV), and thus the stability of these two clusters is approximately equivalent.

The results of $\Delta_2 E$ of $SiMg_n^{\pm 1}$ clusters are shown in **Figure 4C**. One can find that the local strongest peaks are found at $n = 5$, 8, and 10 in $SiMg_n^{-1}$ clusters, while $n = 8$ and 9 in the $SiMg_n^{+1}$ clusters. Naturally, these five clusters are relative more stable than their neighbors. As one knows that HOMO-LUMO gap ($E_{gap}$) value is always responsible for cluster's thermodynamic stability (Aihara, 1999). Notably, there are two kinds of HOMO-LUMO energy gaps, α and β electrons, due to the open-shell structures of $SiMg_n^{\pm 1}$ clusters. As is shown in **Figure 5A** of $SiMg_n^{-1}$ clusters, the local maximum peaks of β-electrons $E_{gap}$ are located at $n = 3$, 8, 9, and 11, while that of α-electrons are at $n = 7$ and 10. **Figure 5B** shows that α-electron of $SiMg_8^{+1}$, β-electrons of $SiMg_3^{+1}$ and $SiMg_9^{+1}$ clusters have local maximum $E_{gap}$ values.

Combing the results of Eb, Ef, $\Delta_2 E$ with $E_{gap}$, the hint toward stability of magic number clusters of $SiMg_n^{\pm 1}$ ($n = 2-12$) is $SiMg_8^{-1}$ and $SiMg_8^{+1}$, or in other words these two clusters
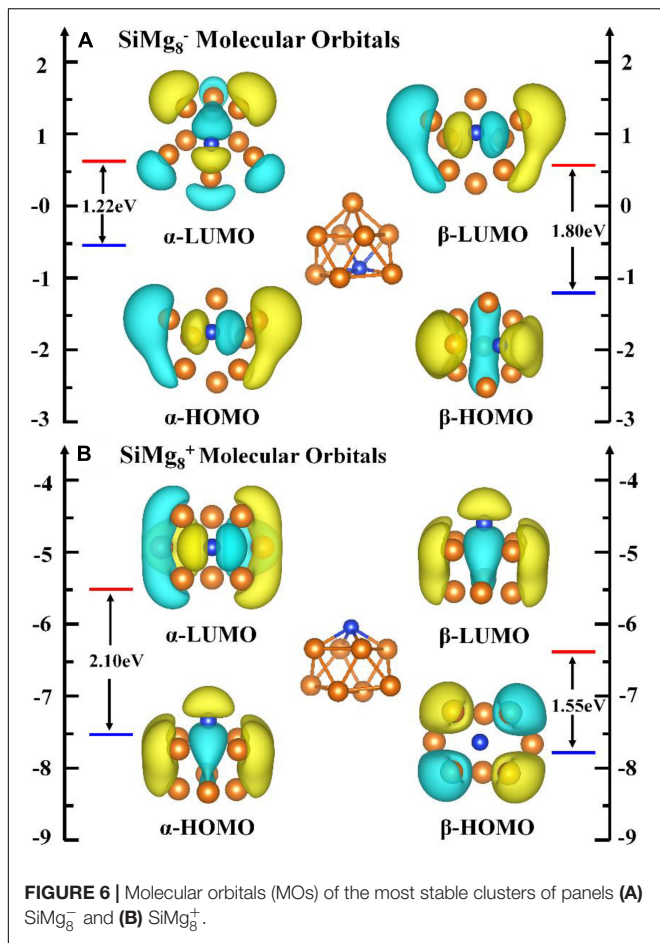
**FIGURE 6 |** Molecular orbitals (MOs) of the most stable clusters of panels **(A)** SiMg$_8^-$ and **(B)** SiMg$_8^+$.

are most stable locally. Interestingly, we have concluded that SiMg$_8^{-1}$ and SiMg$_8^{+1}$ clusters are special ones with tower-like structures in Section "Geometrical Structures of SiMg$_n^{±1}$ Nanosensors." This section's research shows that their structural character probably has strong relationship with their local stability property.

## The Chemical Bonding Analysis of SiMg$_n^{±1}$ Nanosensors

Since the most stable locally SiMg$_8^{-1}$ and SiMg$_8^{+1}$ clusters are found, it is interesting to study the relationship between their stability and chemical bonding. According to the NBO calculations in Section "Geometrical Structures of SiMg$_n^{±1}$ Nanosensors," we can find that SiMg$_8^{+1}$ cluster has C$_S$ symmetry, one SiMg$_2$ unite and six central Mg atoms. While SiMg$_8^{-1}$ cluster has C$_{2V}$ symmetry, one SiMg$_6$ unite and two central Mg atoms. In order to gain insight into their bonding properties, the (α-, β- electron) HOMO, (α-, β- electron) LUMO and top valence molecular orbitals (MOs) are analyzed and are plotted in **Figure 6**. Quantitative composition calculations for chemical bonding show that for SiMg$_8^{-1}$ cluster, α-electron HOMO has a contribution of 15.85% from Si 3p-orbitals, while β-electron HOMO has 30.05% contribution from Si 3p-orbitals. The α-electron HOMO of SiMg$_8^{+1}$ has 24.85% contribution

from Si 3p-orbitals, but β-electron HOMO of SiMg$_8^{+1}$ is mainly composed of Mg 3p-orbitals, or in other words there is nearly no contribution from Si.

To qualitatively study the contribution from silicon atom to chemical bonding in other lower-energy HOMOs of SiMg$_8^{±1}$ clusters, total density of states (TDOS) and partial density of states (PDOS) calculations were performed and were displayed in **Figure 7**. TDOS and PDOS are read (Lu and Chen, 2012a,b):

$$TDOS(E) = \sum_i \delta(E - \varepsilon_i) \qquad (4)$$

$$PDOS_A(E) = \sum_i \Theta_{A,i} F(E - \varepsilon_i) \qquad (5)$$

$\varepsilon_i$ is the energy of molecular orbital $i$ (MO$i$), $\Theta_{A,i}$ is the contribution from part A to MO$i$. Here, part A is Si due to our interesting is how much contribution from Si to the lower-energy HOMOs. As shown in **Figures 7A,B**, the contribution from silicon atoms is always small in the most lower-energy HOMOs (the area to the left of the dotted line). Interestingly, **Figure 7B** shows that there is nearly no contribution from Si to β-electron HOMO of SiMg$_8^{+1}$, which works well with the MOs composition calculations above.

Compared with the research results of the local most stable neutral silicon-doped magnesium clusters (Zhu et al., 2020), we can find some interesting conclusions. First of all, whether silicon-doped magnesium clusters are neutral or charged, their local most stable clusters are composed of one silicon and eight magnesium atoms. Secondly, it is interesting to note that according to our research, SiMg$_8^{0,-1}$ clusters have very similar geometric structures, but the structure of SiMg$_8^{+1}$ has changed a lot. This shows that for neutral silicon-doped magnesium cluster nanosensors, anionization has little effect on its structure, but cationization is not. As we all know that anionic nanoclusters can be used for photoelectron spectra experiments, this conclusion obviously provides a very good guide for future experimental verification.

## The Infrared (IR) and Raman Spectra of SiMg$_n^{±1}$ Nanosensors

In order to be able to experimentally distinguish SiMg$_8^{-1}$ and SiMg$_8^{+1}$ clusters, it is useful to calculate the infrared (IR) and Raman spectra. The Infrared and Raman spectra of SiMg$_8^{±1}$ together with atomic label are shown in **Figure 8**. As shown in **Figure 8A**, the highest intense IR frequency of SiMg$_8^{-1}$ cluster is located at 183 $cm^{-1}$ with Mg7-Si1-Mg8 bonds in-plane tensile vibration. The second and third strongest peaks of SiMg$_8^{-1}$ cluster can be found at 125$cm^{-1}$ and 270$cm^{-1}$. The vibration mode is Si1-Mg4 and Mg7-Mg8 in-bonds tensile vibration, Mg7-Si1-Mg8 bonds in-plane tensile vibration, respectively. **Figure 8C** shows the SiMg$_8^{+1}$ cluster's IR spectra, and two relative strong peaks can be found. The strongest peak is located at 118$cm^{-1}$ with Mg5-Mg4-Mg9-Mg7 out-of-plane wagging vibration of Si1 atom. The second strongest peak at 284$cm^{-1}$ corresponds to Mg9-Si1-Mg5 and Mg7-Si1-Mg4 bond tensile vibration. Three strong vibration peaks can be

**FIGURE 7 |** $\alpha$ - and $\beta$- elections TDOS and PDOS of the most stable clusters of panels **(A)** $SiMg_8^-$ and **(B)** $SiMg_8^+$.



**FIGURE 8 |** The Infrared and Raman spectra of the most stable clusters of panels **(A)** IR for $SiMg_8^-$, **(B)** Raman for $SiMg_8^-$, **(C)** IR for $SiMg_8^+$, and **(D)** Raman for $SiMg_8^+$.
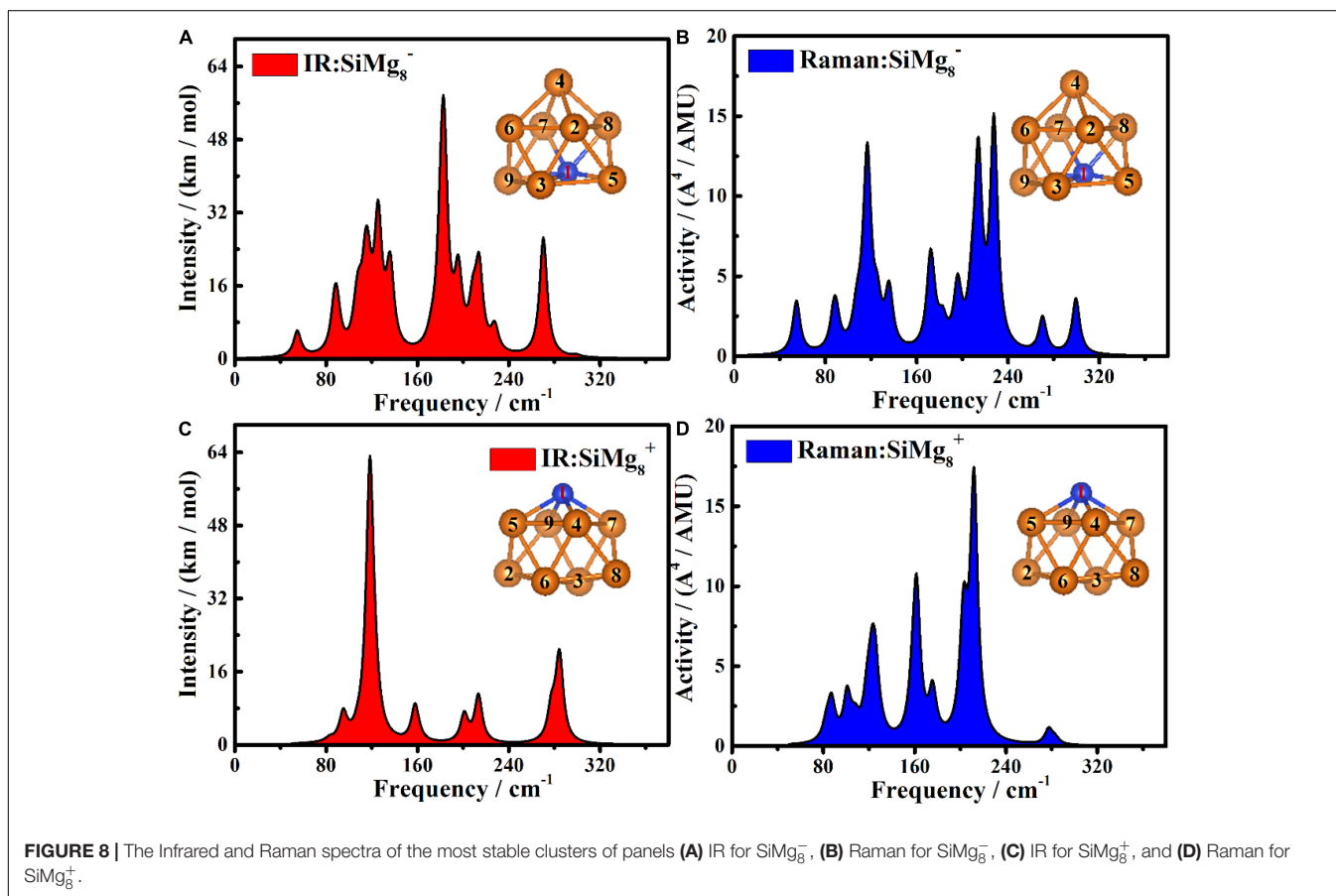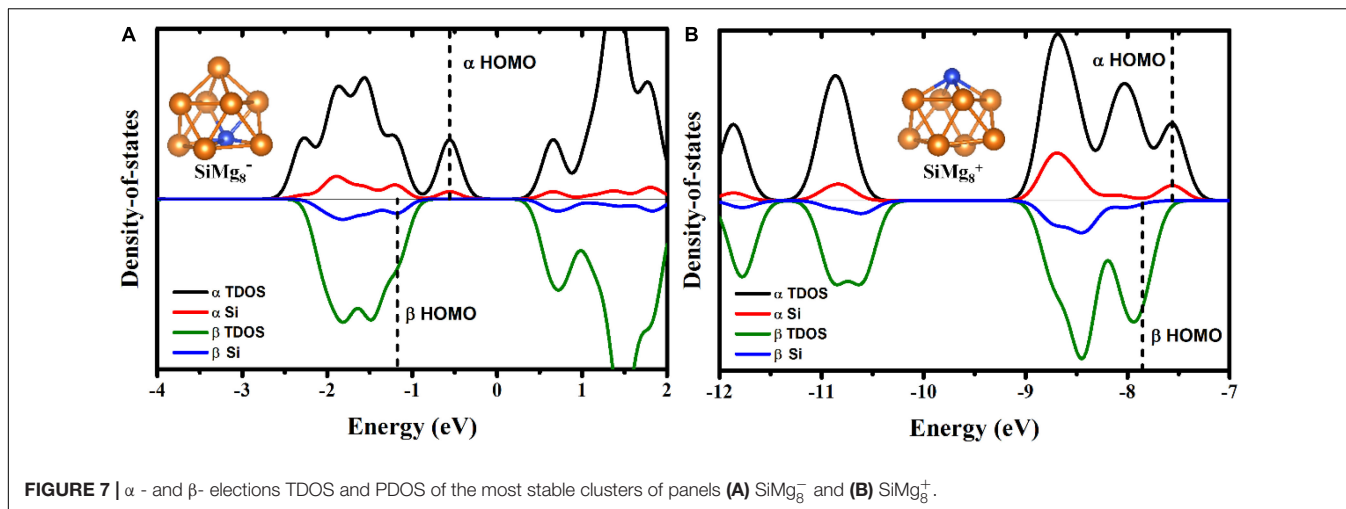
found in **Figure 8B**, which are the Raman spectra of $SiMg_8^{-1}$ cluster. The strongest peak at $227 cm^{-1}$ with total breathing vibration. The second and third strongest Raman frequency at $214 cm^{-1}$ and $116\ cm^{-1}$ correspond to the Si1-Mg4, Mg7-Mg8, Mg9-Mg3-Mg5 in-bonds tensile vibration, Mg9-Si1-Mg5, Mg7-Mg8 bonds out-plane wagging vibration, respectively. **Figure 8D** shows that $SiMg_8^{+1}$ cluster has three strong Raman peaks. The most active Raman frequency at $211 cm^{-1}$ with Mg4–Mg6–Mg5

and Mg7-Mg3-Mg9 bonds in-plane stretching vibration. The other two strong peaks at $161 cm^{-1}$ and $202 cm^{-1}$ resulted from Mg3–Mg5 bond in-plane stretching vibration, Mg4-Mg8–Mg7 and Mg5-Mg2-Mg9 bonds out-of-plane wagging vibration of Si1 atom, respectively.

Overall, the theoretical calculations of infrared (IR) and Raman spectra of $SiMg_8^{-1}$ and $SiMg_8^{+1}$ clusters show that their strongest spectral frequencies are distributed in the range of

$80\text{–}240\ cm^{-1}$. In addition, the strongest infrared spectra difference between $SiMg_8^{-1}$ and $SiMg_8^{+1}$ is close to $65\ cm^{-1}$, thus they can be distinguished experimentally. However, for $SiMg_8^{-1}$ and $SiMg_8^{+1}$, the strongest Raman spectra are relatively close and not easy to distinguish each other.

## CONCLUSION

The stable structures of silicon-doped magnesium nano piezoelectric sensors $SiMg_n^{\pm1}$ ($n = 2-12$), were systematically investigated using the CALYPSO approach coupled with density functional theory. The geometrical growth mechanism of the ground state of $SiMg_n^{\pm1}$ ($n = 2-12$) nanosensors shows that tetrahedral structure ($SiMg_3^{\pm1}$) and tower-like structure ($SiMg_8^{\pm1}$) are two basic structures. Analysis of electronic structural properties reveals the effects of electron transfer and electron configuration on cluster structure formation. Most importantly, clusters relative stability calculations show that $SiMg_8^{\pm1}$ nanosensors have the strongest local stability, and thus can be regarded as candidates for their experimental stable nanostructures. Finally, further studies, such as chemical bonding analysis, infrared and Raman spectra calculations, were performed on these two clusters to in-depth study their stability and experimental identification of operability. We believe that these calculations can play theoretical guiding role in

the development of silicon-doped magnesium nano piezoelectric sensors in future experiments and applications.

## DATA AVAILABILITY STATEMENT

The original contributions presented in the study are included in the article/supplementary material, further inquiries can be directed to the corresponding authors.

## AUTHOR CONTRIBUTIONS

LZ, JZ, and B-CZ wrote a major part of the manuscript. LZ and B-CZ summarized the literature, performed deep review, editing, and supervision. X-FW and M-KL wrote a small part of the manuscript, drawing, and editing. All authors have read and approved the article for publication.

## FUNDING

## REFERENCES

Aihara, J. I. (1999). Reduced HOMO- LUMO gap as an index of kinetic stability for polycyclic aromatic hydrocarbons. *J. Phys. Chem. A* 103, 7487–7495. doi: 10.1021/jp990092i

Becke, A. D. (1988). Density-functional exchange-energy approximation with correct asymptotic behavior. *Phys. Rev. A* 38, 3098–3100. doi: 10.1103/PhysRevA.38.3098

Capitán-Vallvey, L. F., Fernández-Ramos, M. D., Lapresta-Fernández, A., Brunet, E., Rodríguez-Ubis, J. C., and Juanes, O. (2006). Magnesium optical one-shot sensor based on a coumarin chromoionophore. *TALANTA* 68, 1663–1670. doi: 10.1016/j.talanta.2005.08.030

Chen, B. L., Sun, W. G., Kuang, X. Y., Lu, C., Xia, X. X., Shi, H. X., et al. (2018). Structural stability and evolution of medium-sized tantalum-doped boron clusters: a half-sandwich-structured $TaB_{12}^-$ cluster. *Inorganic Chem.* 57, 343–350. doi: 10.1021/acs.inorgchem.7b02585

Delgado, Y. S., Amy, V. M., and Xu, X. J. (2004). "Porous silicon chemical sensors," in *Frontiers of Multifunctional Integrated Nanosystems*, Vol. 152, eds E. Buzaneva and P. Scharff (Dordrecht: Springer), 399–408. doi: 10.1007/1-4020-2173-9_33

Ding, L. P., Zhang, F. H., Zhu, Y. S., Lu, C., Kuang, X. Y., Lv, J., et al. (2015). Understanding the structural transformation, stability of medium-sized neutral and charged silicon clusters. *Sci. Rep.* 5:15951. doi: 10.1038/srep15951

Frisch, M. J., Trucks, G. W., Schlegel, H. B., Scuseria, G. E., Robb, M. A., Cheeseman, J. R., et al. (2009). *Gaussian 09, Revision A.02*. Wallingford CT: Gaussian, Inc.

Guo, W., Fu, M., Zhai, C., and Wang, Z. (2014). Hydrothermal synthesis and gassensing properties of ultrathin hexagonal ZnO nanosheets. *Ceramics Int.* 40, 2295–2298. doi: 10.1016/j.ceramint.2013.07.150

Han, J. G., and Hagelberg, F. A. (2001). Density functional investigation of MoSi$_n$ (n= 1–6) clusters. *J. Mol. Struct. THEOCHEM* 549, 165–180. doi: 10.1016/s0166-1280(01)00493-6

Han, J. G., Xiao, C., and Hagelberg, F. (2002). Geometric and electronic structure of WSi$_n$ (n= 1–6, 12) clusters. *Struct. Chem.* 13, 173–191. doi: 10.1023/a:1015712717153

Han, J. G., Zhao, R. N., and Duan, Y. (2007). Geometries, stabilities, and growth patterns of the bimetal Mo$_2$-doped Si$_n$ (n= 9-16) clusters: a density functional investigation. *J. Phys. Chem. A* 111, 2148–2155. doi: 10.1021/jp0661903

Heidari, I., De, S., Ghazi, S. M., Goedecker, S., and Kanhere, D. G. (2011). Growth and structural properties of Mg$_n$ (n = 10-56) clusters: density functional theory study. *J. Phys. Chem.* 115, 12307–12314. doi: 10.1021/jp204442e

Huber, K. P., and Herzberg, G. (1979). "Constants of diatomic molecules," in *Molecular Spectra and Molecular Structure*, eds K. P. Huber and G. Herzberg (Boston, MA: Springer). doi: 10.1007/978-1-4757-0961-2_2

Jellinek, J., and Acioli, P. H. (2002). Magnesium clusters: structural and electronic properties and the size-induced nonmetal-to-metal transition. *J. Phys. Chem. A* 106, 10919–10925. doi: 10.1021/jp020887g

Jin, Y., Lu, S., Hermann, A., Kuang, X., Zhang, C., Lu, C., et al. (2016). Probing the structural evolution of ruthenium doped germanium clusters: photoelectron spectroscopy and density functional theory calculations. *Sci. Rep.* 6:30116. doi: 10.1038/srep30116

Jin, Y., Tian, Y., Kuang, X. Y., Zhang, C., Lu, C., Wang, J., et al. (2015). Ab initio search for global minimum structures of pure and boron doped silver clusters. *J. Phys. Chem. A* 119, 6738–6745. doi: 10.1021/acs.jpca.5b03542

Köhn, A., Weigend, F., and Ahlrichs, R. (2001). Theoretical study on clusters of magnesium. *Phys. Chem. Chem. Phys.* 3, 711–719. doi: 10.1039/b007869g

Lee, C., Yang, W., and Parr, R. G. (1988). Development of the Colle-Salvetti correlation-energy formula into a functional of the electron density. *Phys. Rev. B* 37, 785–789. doi: 10.1103/PhysRevB.37.785

Li, P. F., Mei, T. T., Lv, L. X., Lu, C., Wang, W. H., Bao, G., et al. (2017). Structure and electronic properties of neutral and negatively charged RhB$_n$ clusters (n = 3-10). *J. Phys. Chem. A* 121, 6510–6516. doi: 10.1021/acs.jpca.7b06123

Lin, J., Yu, T., Han, F., and Yang, G. (2020). Computational predictions of two−dimensional anode materials of metal−ion batteries. *WIREs Comput. Mol. Sci.* 10:e1473. doi: 10.1002/wcms.1473

Lu, C., and Chen, C. (2020a). Indentation-strain stiffening in tungsten nitrides: mechanisms and implications. *Phys. Rev. Mater.* 4:043402. doi: 10.1103/PhysRevMaterials.4.043402

Lu, C., and Chen, C. (2020b). Structure-strength relations of distinct MoN phases from first-principles calculations. *Phys. Rev. Mater.* 2020:044002. doi: 10.1103/PhysRevMaterials.4.044002

Lu, T., and Chen, F. (2012a). Multiwfn: a multifunctional wavefunction analyzer. *J. Comput. Chem.* 33, 580–592. doi: 10.1002/jcc.22885

Lu, T., and Chen, F. (2012b). Quantitative analysis of molecular surface based on improved marching tetrahedra algorithm. *J. Mol. Graph. Model.* 38, 314–323. doi: 10.1016/j.jmgm.2012.07.004

Lv, J., Wang, Y., Zhu, L., and Ma, Y. (2012). Particle-swarm structure prediction on clusters. *J. Chem. Phys.* 137:084104. doi: 10.1063/1.4746757

Pham, V. H., Nguyen, T. V., Nguyen, T. A., Pham, V. D., and Bui, H. (2014). Nano porous silicon microcavity sensor for determination organic solvents and pesticide in water. *Adv. Nat. Sci. Nanosci. Nanotechnol.* 5:045003. doi: 10.1088/2043-6262/5/4/045003

Pradeep, N., Chaitra, V., Uma, V., and Grace, A. N. (2017). Simultaneous growth of magnesium oxide nanowire and nanocubes for gas sensor application. *Sens. Lett.* 15, 413–418. doi: 10.1166/sl.2017.3791

Reed, A. E., Curtiss, L. A., and Weinhold, F. (1988a). Intermolecular interactions from a natural bond orbital, donor-acceptor viewpoint. *Chem. Rev.* 88, 899–926. doi: 10.1021/cr00088a005

Reed, A. E., Weinstock, R. B., and Weinhold, F. (1988b). Natural population analysis. *J. Chem. Phys.* 83, 735–746. doi: 10.1063/1.449486

Ruette, F., Saìnchez, M., Anez, R., Bermúdez, A., and Sierraalta, A. (2005). Diatomic molecule data for parametric methods. *J. Mol. Struct. THEOCHEM* 729, 19–37. doi: 10.1016/j.theochem.2005.04.024

Shao, X., Qu, X., Liu, S., Yang, L., Yang, J., Liu, X., et al. (2019). Structure evolution of chromium-doped boron clusters: toward the formation of endohedral boron cages. *RSC Adv.* 9, 2870–2876. doi: 10.1039/C8RA09143A

Shukla, S. K., Parashar, G. K., Mishra, A. P., Misra, P., Yadav, B. C., Shukla, R. K., et al. (2004). Nano-like magnesium oxide films and its significance in optical fiber humidity sensor. *Sens. Actuat. B Chem.* 98, 5–11. doi: 10.1016/j.snb.2003.05.001

Sun, Y., Lv, J., Xie, Y., Liu, H., and Ma, Y. (2019). Route to a superconducting phase above room temperature in electron-doped hydride compounds under high pressure. *Phys. Rev. Lett.* 123:097001. doi: 10.1103/physrevlett.123.097001

Wang, J., Li, X., Wei, B., Sun, R., Yu, W., Hoh, H. Y., et al. (2020). Activating basal planes of $NiPS_3$ for hydrogen evolution by nonmetal heteroatom doping. *Adv. Funct. Mater.* 30:1908708. doi: 10.1002/adfm.201908708

Wang, J. W., Yao, Z. S., and Poon, A. W. (2015). Silicon-nitride-based integrated optofluidic biochemical sensors using a coupled-resonator optical waveguide. *Front. Mater.* 2:34. doi: 10.3389/fmats.2015.00034

Wang, Y., Lv, J., Zhu, L., and Ma, Y. (2010). Crystal structure prediction via particle-swarm optimization. *Phys. Rev. B* 82:094116. doi: 10.1103/physrevb.82.094116

Wang, Y., Lv, J., Zhu, L., and Ma, Y. (2012). CALYPSO: a method for crystal structure prediction. *Comput. Phys. Commun.* 183, 2063–2070. doi: 10.1016/j.cpc.2012.05.008

Xia, X., Kuang, X., Lu, C., Jin, Y., Xing, X. D., Merino, G., et al. (2016). Deciphering the structural evolution and electronic properties of magnesium clusters: an aromatic homonuclear metal. *J. Phys. Chem. A* 120, 7947–7954. doi: 10.1021/acs.jpca.6b07322

Zeng, W., Liu, T., and Wang, Z. (2012). Impact of Nb doping on gas-sensing performance of $TiO_2$ thick-film sensors. *Sens. Actuat. B Chem.* 166–167, 141–149. doi: 10.1016/j.snb.2012.02.016

Zhang, F. G., Zhang, H. R., Xin, W., Chen, P., Hu, Y. F., Zhang, X. Y., et al. (2020). Probing the structural evolution and electronic properties of divalent metal Be2Mgn clusters from small to medium-size. *Sci. Rep.* 10:6052. doi: 10.1038/s41598-020-63237-8

Zhao, L., Qu, X., Wang, Y., Lv, J., and Ma, Y. (2017). Effects of manganese doping on the structure evolution of small-sized boron clusters. *J. Phys. Condens. Matter* 29:265401. doi: 10.1088/1361-648X/aa7190

Zhao, Y. R., Bai, T. T., Jia, L. N., Xin, W., Hu, Y. F., Zheng, X. S., et al. (2019). Probing the structural and electronic properties of neutral and anionic lanthanum-doped silicon clusters. *J. Phys. Chem. C* 123, 28561–28568. doi: 10.1021/acs.jpcc.9b07184

Zhu, B., Zhang, S., and Zeng, L. (2020). The effect of silicon doping on the geometrical structures, stability, and electronic and spectral properties of magnesium clusters: DFT study of SiMg$_n$ (n = 1−12) clusters. *Int. J. Quant. Chem.* 120:e26143. doi: 10.1002/qua.26143